Proceedings of the International Conference on Oxide Materials for Electronic Engineering, May 29–June 2, 2017, Lviv

Synthesis and Vibration Spectroscopy of Nano-Sized Manganese Oxides

N. Mironova-Ulmane[a,*], A. Kuzmin[a], V. Skvortsova[a], G. Chikvaidze[a], I. Sildos[b], J. Grabis[c], D. Jankovičа[c], A. Dindune[c] and M. Maiorov[d]

[a]Institute of Solid State Physics, University of Latvia, Kengaraga Str. 8, LV-1063 Riga, Latvia
[b]Institute of Physics, University of Tartu, W. Ostwaldi tn 1, 50411 Tartu, Estonia
[c]Institute of Inorganic Chemistry, Riga Technical University, P. Valdena Str. 3/7, LV-1048 Riga, Latvia
[d]Institute of Physics, University of Latvia, Miera Str. 32, LV-2169 Salaspils, Latvia

X-ray diffraction, micro-Raman and the Fourier transform infrared spectroscopies as well as magnetometry measurements were performed on nanosized manganese oxides to probe their phase composition and magnetic properties. It was shown that the XRD method is less sensitive to phase composition of manganese oxide samples than spectroscopic methods. While in some samples the XRD method recognised only the manganosite MnO phase, the Raman and FT-IR methods revealed additionally the presence of the hausmannite Mn_3O_4 phase.

DOI: 10.12693/APhysPolA.133.1013
PACS/topics: 81.07.Wx, 61.05.cp, 78.30.Hv, 75.30.Cr

1. Introduction

Manganese oxides are widely used as supercapacitor electrode materials [1] and catalysts [2], for the preparation of Li–Mn–O electrodes for rechargeable lithium batteries [3, 4] and of soft magnetic materials such as manganese zinc ferrite, which is applicable as magnetic cores in transformers for power supplies [5]. The manganosite MnO phase (space group $Fm3m$) is a Mott insulator ordering antiferromagnetically below approximately 118 K [6]. Magnetostructural phase transitions in MnO antiferromagnets were studied by high-precision neutron diffraction [7]. It was shown that the structural and magnetic transitions in polycrystalline MnO occur synchronously, and their temperatures coincide within the experimental errors: $T_{str} \approx T_{mag} \approx (119 \pm 1)$ K [7]. While being studied for a long time, MnO still attracts considerable interest, which has been extended recently to its nanostructures [8, 9]. It is known that the magnetic properties of MnO are strongly affected by the presence of Mn_3O_4 impurity phase, being ferrimagnetic below approximately 43 K [10]. Mn_3O_4 has the normal spinel structure with general formula $A^{2+}B_2^{3+}O_4^{2-}$. At room temperature, it has tetragonal hausmannite (space group $I4_1/amd$) phase with Mn^{3+} and Mn^{2+} ions occupying the octahedral (B-sites) and tetrahedral (A-sites) positions of the spinel structure, respectively. The MnO_6 octahedra are tetragonally distorted due to the Jahn–Teller effect on Mn^{3+} ions [11]. Thus, the ionic formula of Mn_3O_4 is often written in spinel notation as $Mn^{2+}[Mn_2^{3+}]O_4$.

In this study the sensitivity of several experimental methods as X-ray diffraction (XRD), micro-Raman and Fourier transform infrared (FT-IR) spectroscopies as well as magnetometry measurements to the presence of Mn_3O_4 impurity in manganosite MnO phase was investigated.

2. Experimental

The manganese oxides nanoparticles were synthesized by hydrothermal method. 0.5 M of cetyltrimethylammonium bromide (CTAB) was dissolved in 80 ml of ethanol. The CTAB buffer extraction was done immediately before use since it is required that the buffer should be freshly prepared. Next, the manganese acetate was added and dissolved. After that glycerol and nitric acid were added at the temperature of 350 K, stirred by magnetic stirrer and evaporated completely. The resulting powder product was loaded in a preheated to 620 °C furnace and heated at 720 °C for 2 h in a vacuum. As a result, the first sample, labelled as MnO(I), was obtained. The second sample, labelled as MnO(II), was obtained by heating at 720 °C for 2 h in a mixed argon and hydrogen atmosphere instead of vacuum.

The XRD patterns of the nanosized powders were recorded at room temperature using a Bruker ADVANCE D8 θ–2θ diffractometer equipped with a copper anode tube (Cu K_α radiation) in the range of $2\theta = 10$–$100°$ with the angular step size 0.01° and the scan speed 0.3°/min.

Micro-Raman scattering spectra were measured in the backscattering geometry at room temperature through 20× and 50× objectives using a Renishaw inVia micro-Raman spectrometer equipped with an argon laser (488 nm, maximal cw power $P_{ex} = 50$ mW) and through 40× objective using a confocal spectrometer Nanofinder-S (SOLAR TII, Ltd.) equipped with a DPSS laser

*corresponding author; e-mail: nina@cfi.lu.lv

(532 nm, maximal cw power P_{ex} = 150 mW). The spectral signal was dispersed by 2400 or 600 grooves/mm gratings onto Peltier-cooled CCD detectors.

Infrared spectra were measured using the KBr pellet method in the energy range from 200 to 800 cm^{-1} employing a vacuum FT-IR Bruker VERTEX 80v spectrometer equipped with a closed-circle optical helium cryostat.

The temperature dependences of the oxide magnetic properties (specific susceptibility) were measured using a vibrating sample magnetometer (Lake Shore Cryotronic Co., Model 7404 VSM) equipped with the single-stage variable temperature option.

3. Results and discussion

The crystallinity and phase composition of both MnO(I) and MnO(II) samples were investigated by X-ray powder diffraction. Their XRD patterns are shown in Fig. 1. The XRD pattern of MnO(I) corresponds to a pure face-centred cubic MnO phase (mineralogical name manganosite, JCPDS Card 00-075-1090), which is isostructural with NaCl. No additional peaks due to any impurity phase are observed. The obtained lattice parameter of MnO is a = 4.46 Å, and the average crystallite size is 55 nm. The peaks in the XRD pattern of MnO(II) sample are broader than for MnO(I) sample due to smaller average crystallite size, and, additionally, the XRD pattern contains a contribution from impurity phase Mn_3O_4 (mineralogical name hausmannite). The lattice parameters of MnO-manganosite (average crystallite size is 22 nm) and Mn_3O_4-hausmannite (average crystallite size is 14 nm) phases in MnO(II) sample agree well with those for bulk crystals: a = 4.45 Å (JCPDS Card 00-075-1090) and a = 5.7621 Å, c = 9.4696 Å (JCPDS Card 01-080-0382), respectively.

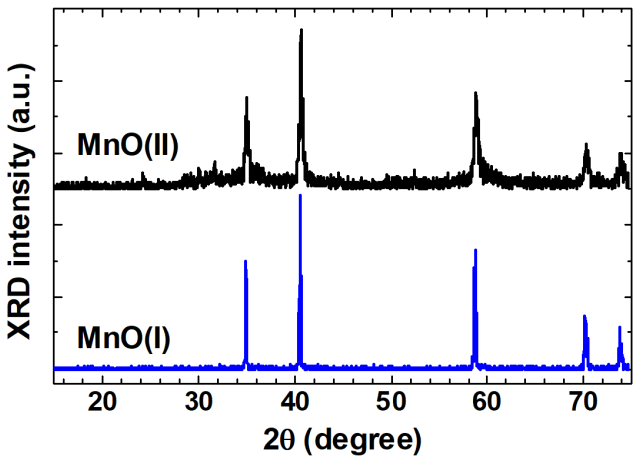

Fig. 1. X-ray diffraction patterns of manganese oxide samples.

Micro-Raman scattering spectra of MnO(I) and MnO(II) samples are shown in Fig. 2. Pure MnO has at room temperature the cubic rock-salt structure, and, thus, it should not exhibit any first-order Raman activity. The Raman scattering spectra of both samples contain a strong narrow band at 660 cm^{-1} and two small bands at about 318 and 370 cm^{-1}, indicating the presence of hausmannite Mn_3O_4 phase [11–14]. Detailed assignments of theoretically computed Raman modes of Mn_3O_4 can be found in [11]. The Raman spectrum of MnO(I) sample contains additionally two broad asymmetric bands at about 530 and 1050 cm^{-1}. The low frequency band at 530 cm^{-1} has been attributed previously to 2TO [15, 16] or LO [17] phonons in manganosite MnO phase. The high frequency band at 1050 cm^{-1} has complex origin: it envelops two bands related to the TO+LO (a band wing at 950 cm^{-1}) and 2LO modes [17] in manganosite MnO phase. The intermediate band due to the 2TO modes has a weak intensity and is masked by a narrow band contribution at 660 cm^{-1} due to the Mn_3O_4 phase. Such assignments agree well with the results of the inelastic neutron scattering [18] and recent first-principles theoretical calculations [19], which give the zone-centre phonon modes ω(TO) $\approx$ 280 cm^{-1} and ω(LO) $\approx$ 497 cm^{-1}. The obtained results also agree with those for single-crystal MnO and Mn_3O_4 samples [17], which were epitaxially grown by the chemical transport reactions method from polycrystalline MnO source on MgO (100) substrate.

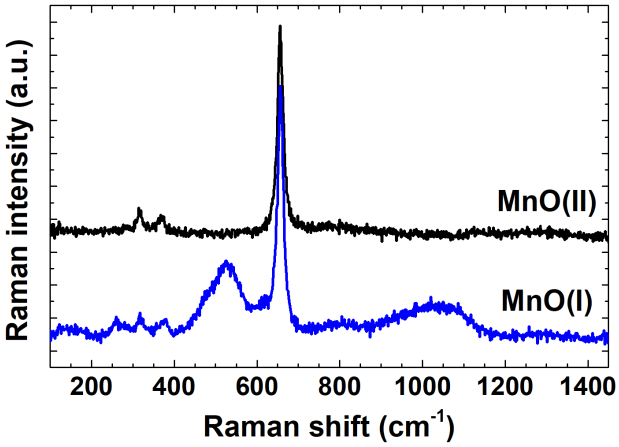

Fig. 2. Micro-Raman scattering spectra of manganese oxide samples.

The infrared spectra of MnO(I) and MnO(II) samples in the far-red range of 230–650 cm^{-1} are shown in Fig. 3 and are composed of several strongly overlapped bands. The spectrum of MnO(I) sample consists of a broad band at 285 cm^{-1} attributed to manganosite MnO phase, and four bands at 420, 480, 510, and 600 cm^{-1} attributed to hausmannite Mn_3O_4 phase [11, 20]. The spectrum of MnO(II) sample consists of three main bands at 257, 382, and 490 cm^{-1} and two weak bands at 434 and 602 cm^{-1}, which can be attributed to hausmannite Mn_3O_4 phase [11, 20]. Note that three bands at 407, 502, and 620 cm^{-1} were reported in the literature for 10 nm Mn_3O_4 nanoparticles [13].

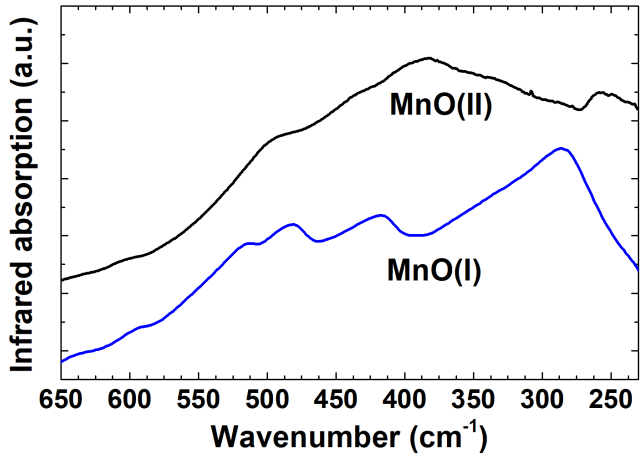

Fig. 3. Infrared spectra of manganese oxide samples.

The magnetic properties of MnO(I) and MnO(II) samples were investigated by magnetometry measurements. Magnetic susceptibility of an antiferromagnet should increase with temperature rise up to the Néel temperature and then decrease following the Curie–Weiss law. The temperature dependences of the magnetic susceptibility for both nanocrystalline samples are shown in Fig. 4: they have a particular behaviour at 120 K, corresponding to the Néel temperature of manganosite MnO. However, temperature dependences for both samples do not follow the expected one for pure MnO [21]. The behaviour of magnetic susceptibility deviates from the expected one below the Néel temperature for MnO(I) sample and at all temperatures for MnO(II) sample. Such behaviour is evidently due to the presence of the hausmannite Mn_3O_4 phase.

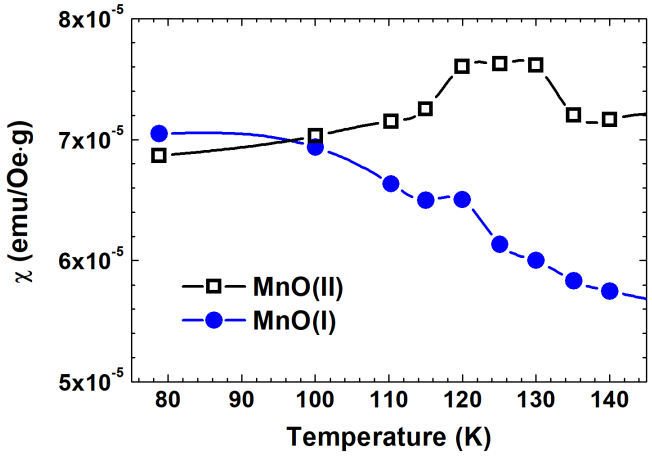

Fig. 4. Temperature dependence of the specific susceptibility of manganese oxide samples.

4. Conclusions

Nanocrystalline MnO samples with the average crystallite size of 22 and 55 nm were synthesized by hydrothermal method and studied by X-ray diffraction, micro-Raman and FT-IR spectroscopies to evaluate their structure and phase composition. The magnetic properties of samples were probed by magnetometry measurements.

Our results indicate that impurity hausmannite Mn_3O_4 phase is always present in the samples but its amount can be controlled by choosing annealing atmosphere. In particular, the annealing of manganese oxide in vacuum leads to significantly reduced amount of Mn_3O_4 phase, which is not observed by XRD but is detectable by Raman and FT-IR methods. At the same time, the annealing in mixed argon and hydrogen atmosphere results in a larger amount of impurity Mn_3O_4 phase, which can be detected also by XRD. Thus, we have shown that the Raman and FT-IR spectroscopies are more sensitive to the presence of Mn_3O_4 phase than X-ray diffraction method.

The transition from the antiferromagnetic state to the paramagnetic state was observed for both nanocrystalline MnO(I) and MnO(II) samples using the magnetic susceptibility measurements at the temperature of 120 K, which corresponds to the Néel temperature of manganosite.

Acknowledgments

The present study has been supported by the Latvian National Research Program IMIS2. One of us, IS, was supported by MES RF RFMEFI61615X0064.

References

[1] L. Zhang, T. Wei, W. Wang, X.S. Zhao, *Micropor. Mesopor. Mater.* **123**, 260 (2009).

[2] V. Iablokov, K. Frey, O. Geszti, N. Kruse, *Catal. Lett.* **134**, 210 (2010).

[3] A.R. Armstrong, P.G. Bruce, *Nature* **381**, 499 (1996).

[4] N. Yabuuchi, S. Komaba, *Sci. Technol. Adv. Mater.* **15**, 043501 (2014).

[5] S.E. Jacobo, S. Duhalde, H.R. Bertorello, *J. Magn. Magn. Mater.* **272-276**, 2253 (2004).

[6] C.G. Shull, J.S. Smart, *Phys. Rev.* **76**, 1256 (1949).

[7] A.M. Balagurov, I.A. Bobrikov, S.V. Sumnikov, V.Yu. Yushankhai, N. Mironova-Ulmane, *JETP Lett.* **104**, 88 (2016).

[8] W.-M. Chen, L. Qie, Y. Shen, Y.-M. Sun, L.-X. Yuan, X.-L. Hu, W.-X. Zhang, Y.-H. Huang, *Nano Energy* **2**, 412 (2013).

[9] J. Feng, Y. Liang, H. Wang, Y. Li, B. Zhang, J. Zhou, J. Wang, T. Regier, H. Dai, *Nano Res.* **5**, 718 (2012).

[10] A.E. Berkowitz, G.F. Rodriguez, J.I. Hong, K. An, T. Hyeon, N. Agarwal, D.J. Smith, E.E. Fullerton, *Phys. Rev. B* **77**, 024403 (2008).

[11] T. Larbi, K. Doll, T. Manoubi, *J. Alloys Comp.* **688**, 692 (2016).

[12] F. Buciuman, F. Patcas, R. Craciun, D.R.T. Zahn, *Phys. Chem. Chem. Phys.* **1**, 185 (1999).

[13] X. Li, L. Zhou, J. Gao, H. Miao, H. Zhang, J. Xu, *Powder Technol.* **190**, 324 (2009).

[14] M. Ristic, S. Music, S. Popovic, D.J. Dragčevic, M. Marciuš, M. Ivanda, *J. Mol. Struct.* **1044**, 255 (2013).

[15] H.-H. Chou, H.Y. Fan, *Phys. Rev. B* **13**, 3924 (1976).

[16] Y. Mita, Y. Sakai, D. Izaki, M. Kobayashi, S. Endo, S. Mochizuki, *Phys. Status Solidi B* **223**, 247 (2001).

[17] N. Mironova-Ulmane, A. Kuzmin, M. Grube, *J. Alloys Comp.* **480**, 97 (2009).

[18] E.M.L. Chung, D. McK. Paul, G. Balakrishnan, M.R. Lees, A. Ivanov, M. Yethiraj, *Phys. Rev. B* **68**, 140406 (2003).

[19] U.D. Wdowik, D. Legut, *J. Phys. Condens. Matter* **21**, 275402 (2009).

[20] C.M. Julien, M. Massot, C. Poinsignon, *Spectrochim. Acta A* **60**, 689 (2004).

[21] T.R. Mcguire, R.J. Happel, *J. Phys. Rad.* **20**, 424 (1959).

Institute of Solid State Physics, University of Latvia as the Center of Excellence has received funding from the European Union's Horizon 2020 Framework Programme H2020-WIDESPREAD-01-2016-2017-TeamingPhase2 under grant agreement No. 739508, project CAMART²